Supporting Information

High-Efficiency and Thermal/Moisture Stable $CsPbI_{2.84}Br_{0.16}$ Inorganic Perovskite Solar Cells Enabled by a Multifunctional Cesium Trimethylacetate Organic Additive

*Hang Zhao [a,b], Yao Fu [a,b], Zhenzhen Li [a,b], Shujie Yang [a,b], Baomin Xu[c], Xiaolong Liu [a,b], Jia Xu [a,b], Shengzhong (Frank) Liu [d], Jianxi Yao [a,b]**

[a] *State Key Laboratory of Alternate Electrical Power System with Renewable Energy Sources, North China Electric Power University, Beijing 102206, China.*
[b] *Beijing Key Laboratory of Energy Safety and Clean Utilization, North China Electric Power University, Beijing 102206, China.*
[c] *Department of Materials Science and Engineering, Southern University of Science and Technology, Shenzhen, Guangdong Province, 518055 China; Shenzhen Engineering Research and Development Center for Flexible Solar Cells, Southern University of Science and Technology, Shenzhen, Guangdong Province, 518055 China*
[d] *Key Laboratory of Applied Surface and Colloid Chemistry, National Ministry of Education; Shaanxi Key Laboratory for Advanced Energy Devices; Shaanxi Engineering Lab for Advanced Energy Technology; Institute for Advanced Energy Materials; School of Materials Science and Engineering, Shaanxi Normal University, Xi'an 710119, China.*

** Corresponding authors' E-mails: jianxiyao@ncepu.edu.cn*

Supporting Figures and Tables

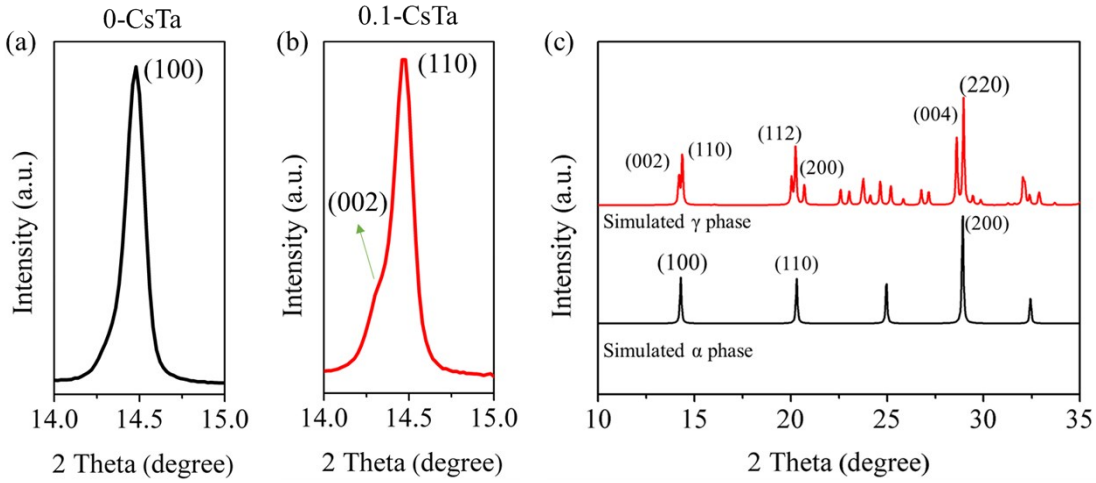

Figure S1. (a) The enlarged view of the (100) peak for a 0-CsTa film. (b) The enlarged view of the (002) and (110) peaks for a 0.1-CsTa film. (c) The simulated XRD patterns for the α and γ phases.

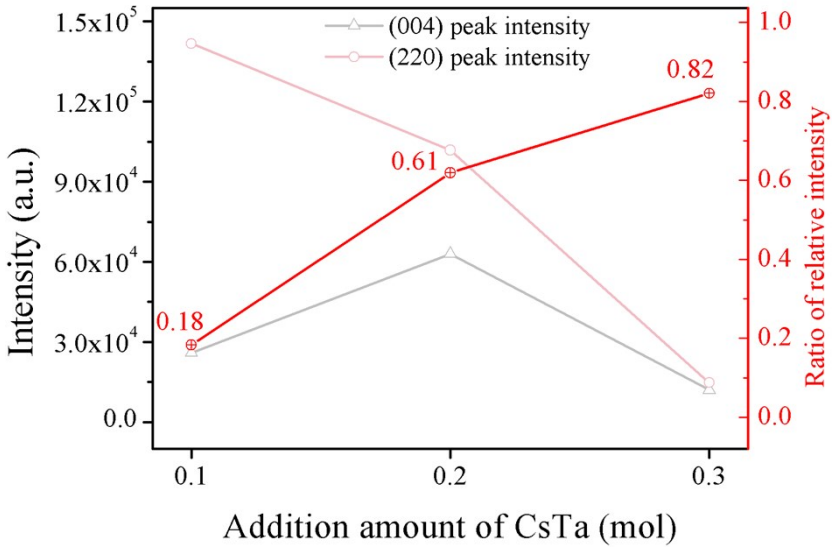

Figure S2. The (004) and (220) peak intensities for 0.1-CsTa, 0.2-CsTa and 0.3-CsTa films. The red line shows the ratio of the (004) peak intensity to the (220) peak intensity for 0.1-CsTa, 0.2-CsTa and 0.3-CsTa films.

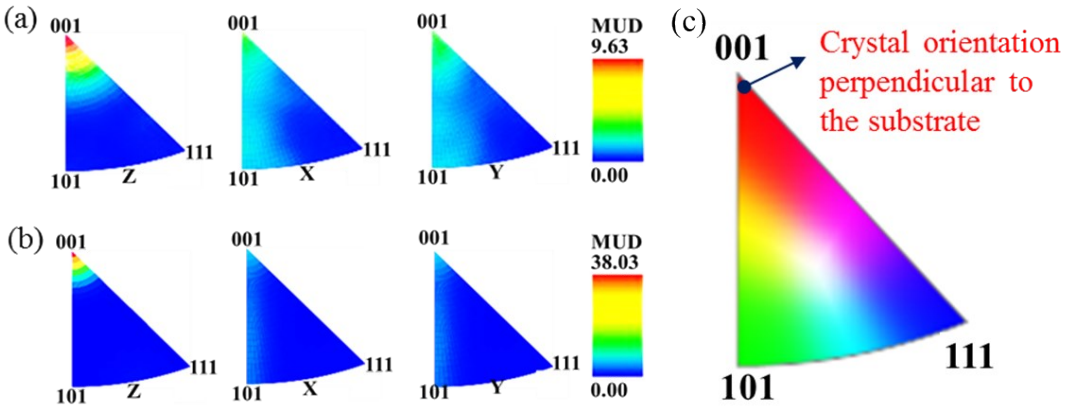

Figure S3. The corresponding inverse pole figures for (a) 0-CsTa and (b) 0.1-CsTa films. (c) The color key (inserted in Figure 1d) varies with the orientation of the crystal. The red color in the coordinate represents the growth orientation perpendicular to the substrate. The other colors represent the growth in the other directions.

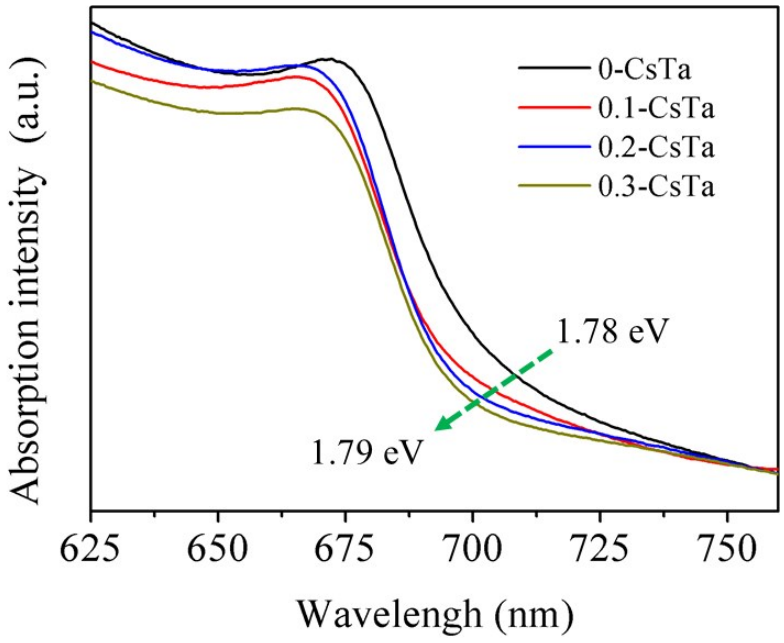

Figure S4. The UV-Vis spectra for n-CsTa $CsPbI_{2.84}Br_{0.16}$ perovskite films.

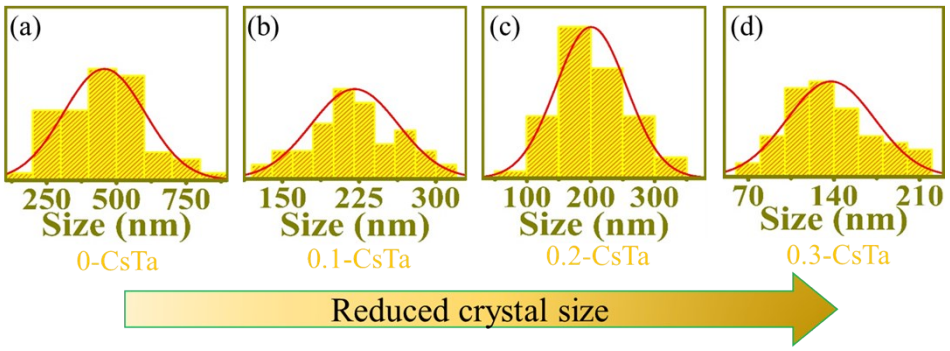

Figure S5. The size distribution of the crystals in n-CsTa films determined by counting 50 crystal grains. (a) 0-CsTa. (b) 0.1-CsTa. (c) 0.2-CsTa. (d) 0.3-CsTa.

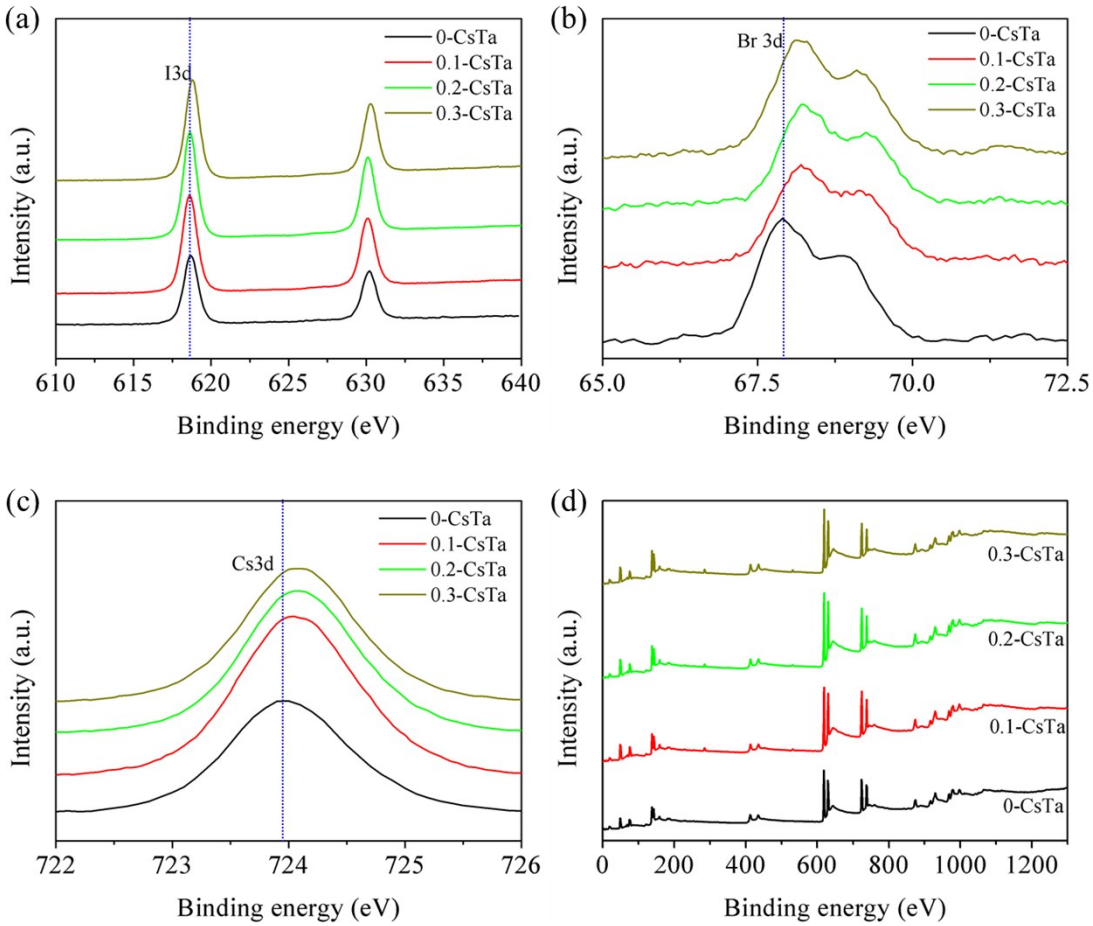

Figure S6. The binding energies for (a) I 3d, (b) Br 3d and (c) Cs 3d for n-CsTa films tested with XPS. (d) The survey curves for the XPS spectra.

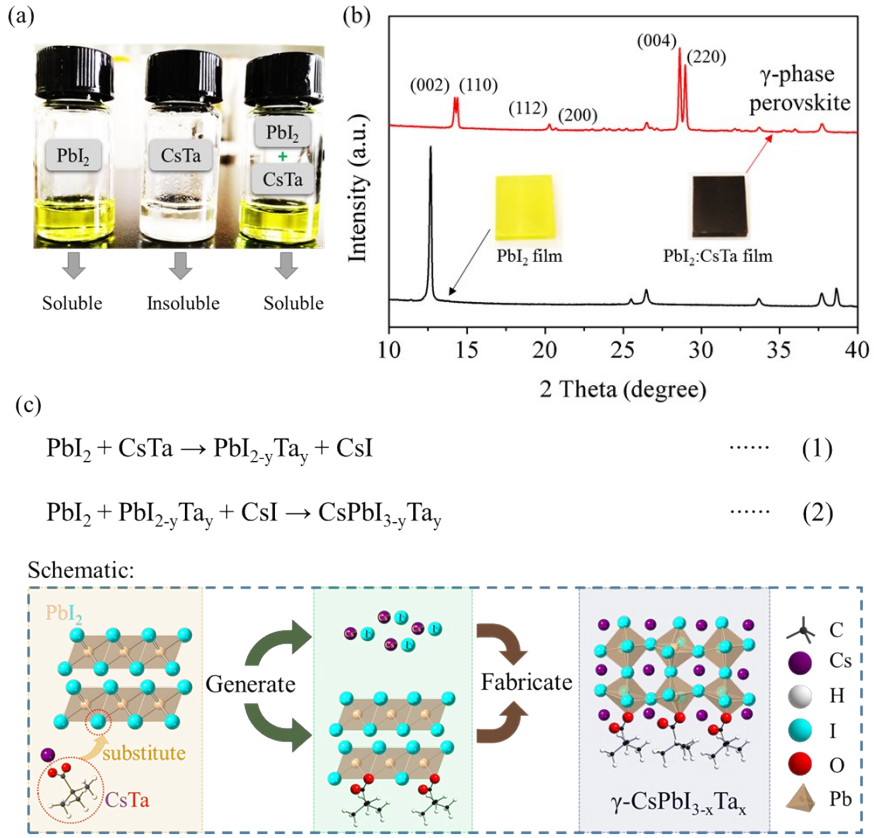

Figure S7. (a) Images for the solubility of PbI_2, CsTa and PbI_2/CsTa mixture powders in DMSO. (b) XRD patterns for films obtained from PbI_2 and PbI_2/CsTa precursor solutions. The black film preparation processes: PbI_2/CsTa precursor solution was spin-coated on a 150°C preheated substrate. Then the black film was obtained by annealing the wet-fresh film at 105°C. (c) The reaction processes and the schematic for γ-phase perovskite formation in PbI_2/CsTa case.

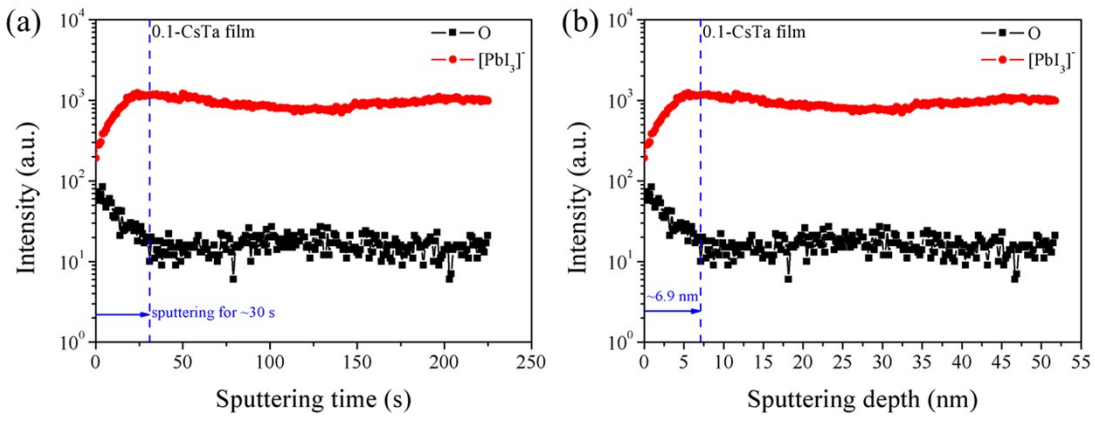

Figure S8. The intensity-sputtering time and intensity-sputtering depth profiles for the O element and $[PbI_3]^-$ in 0.1-CsTa films. Sputtering rate: 0.23 nm/s.

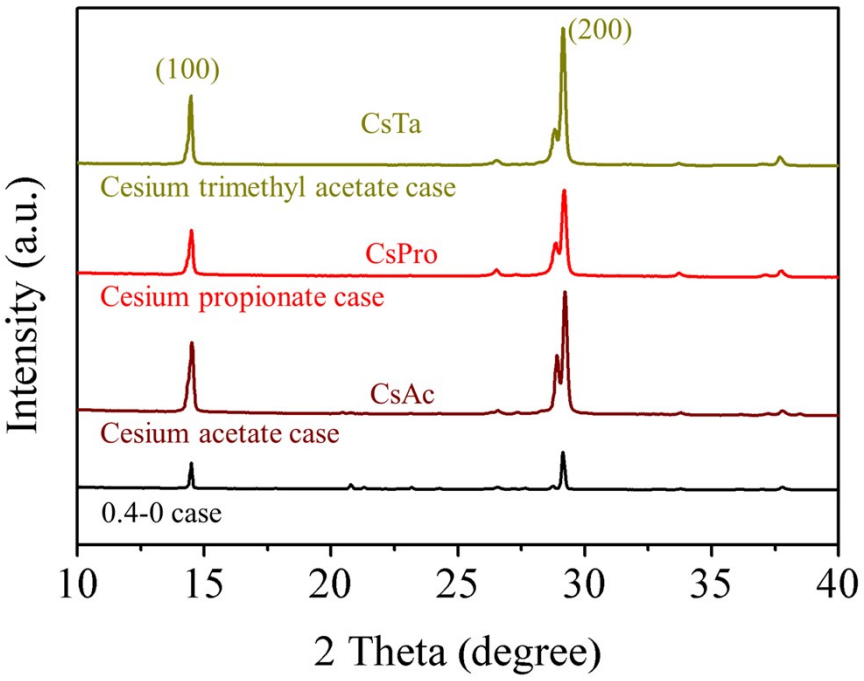

Figure S9. The XRD patterns for 0.1-CsAc, 0.1-CsPro and 0.1-CsTa films. The black line shows the XRD data for the 0-CsTa perovskite film.

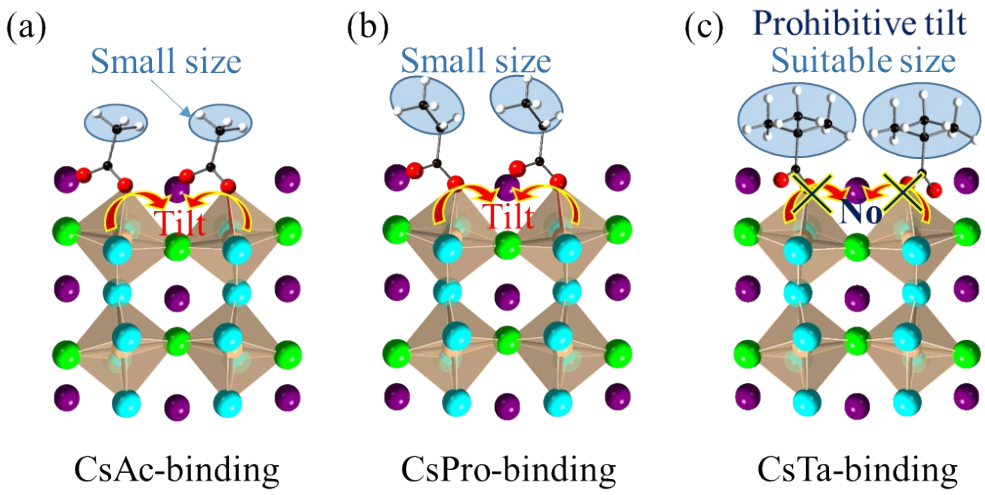

Figure S10. The schematics for the blocking effect due to the terminal groups in CsAc, CsPro and CsTa on the stability of the perovskite structure.

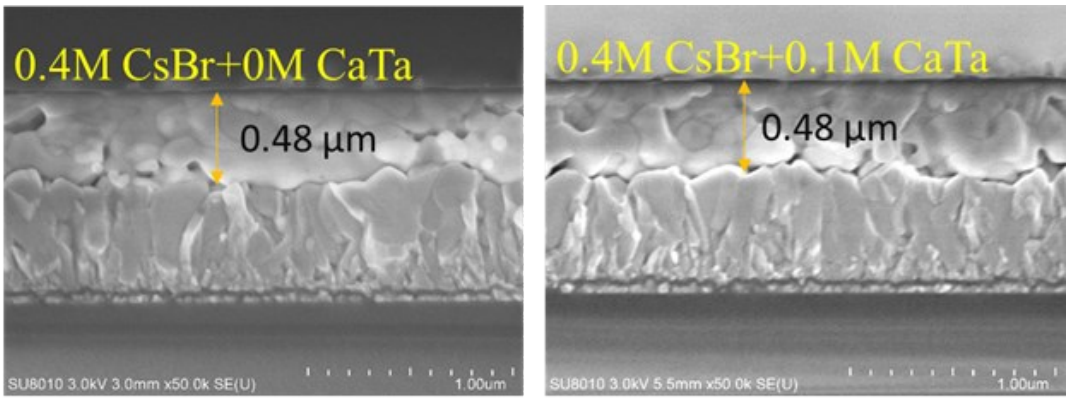

Figure S11. The cross-section SEM images for 0-CsTa and 0.1-CsTa $CsPbI_{2.84}Br_{0.16}$ perovskite films.

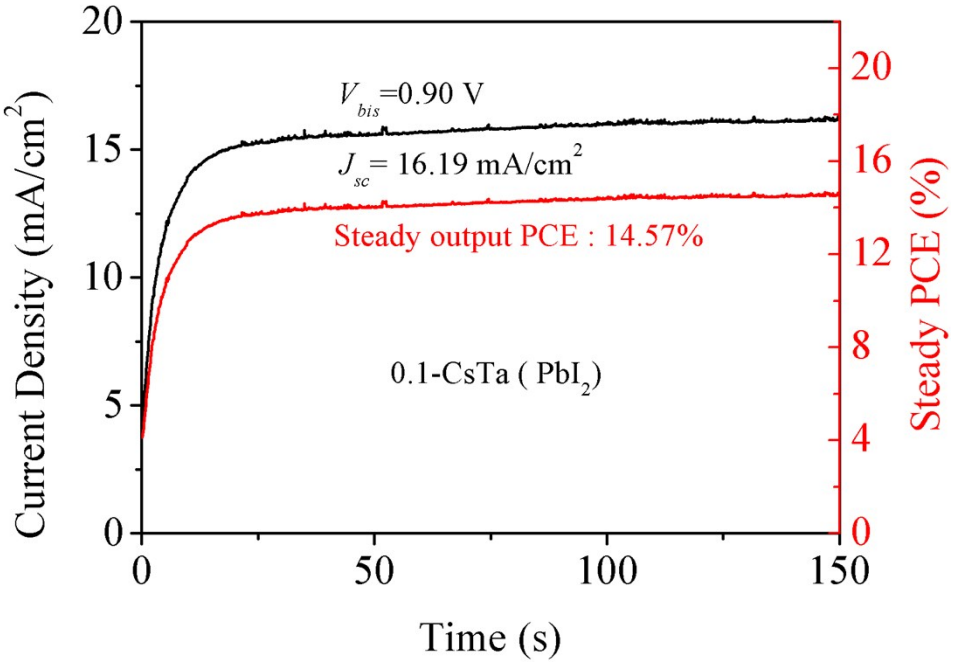

Figure S12. The steady output current densities at the maximum PCE points for 0.1-CsTa devices based on the use of PbI_2 as the lead source.

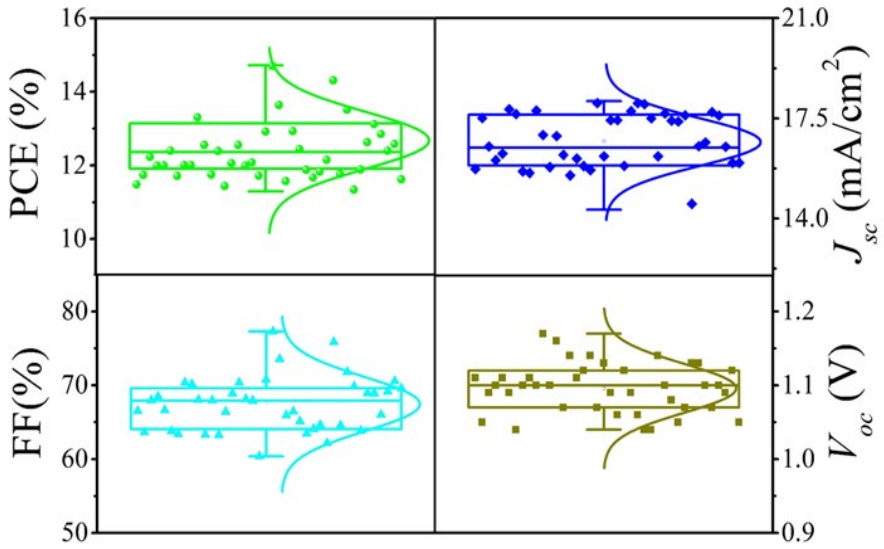

Figure S13. The statistical photoelectric parameters for 0.1-CsTa PSCs (40 devices).

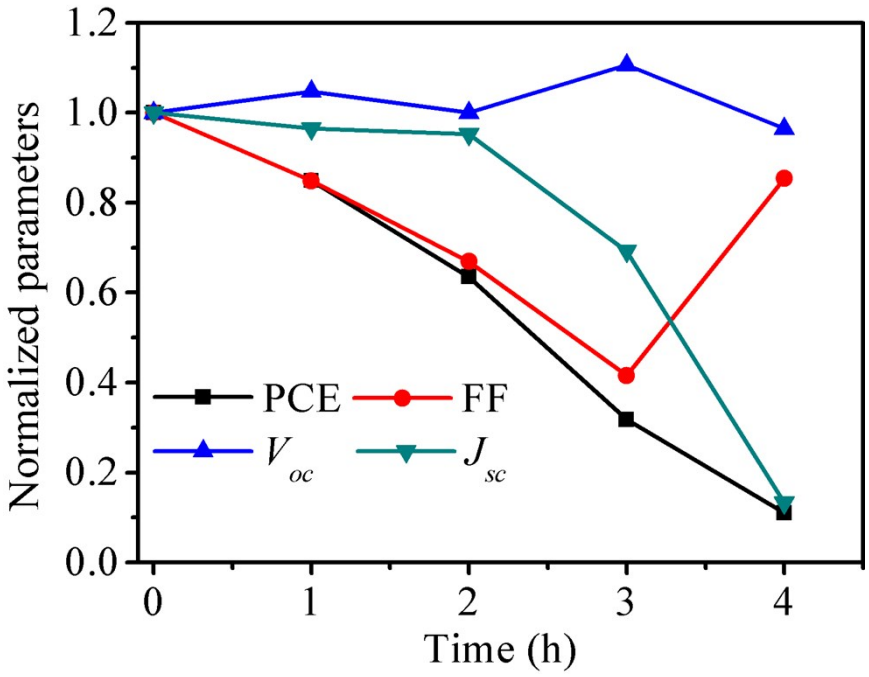

Figure S14. Photovoltaic parameter decays for PbI_2-prepared 0-CsTa PSCs for environmental stability testing in air (RH: ~20%, RT: 10°C).

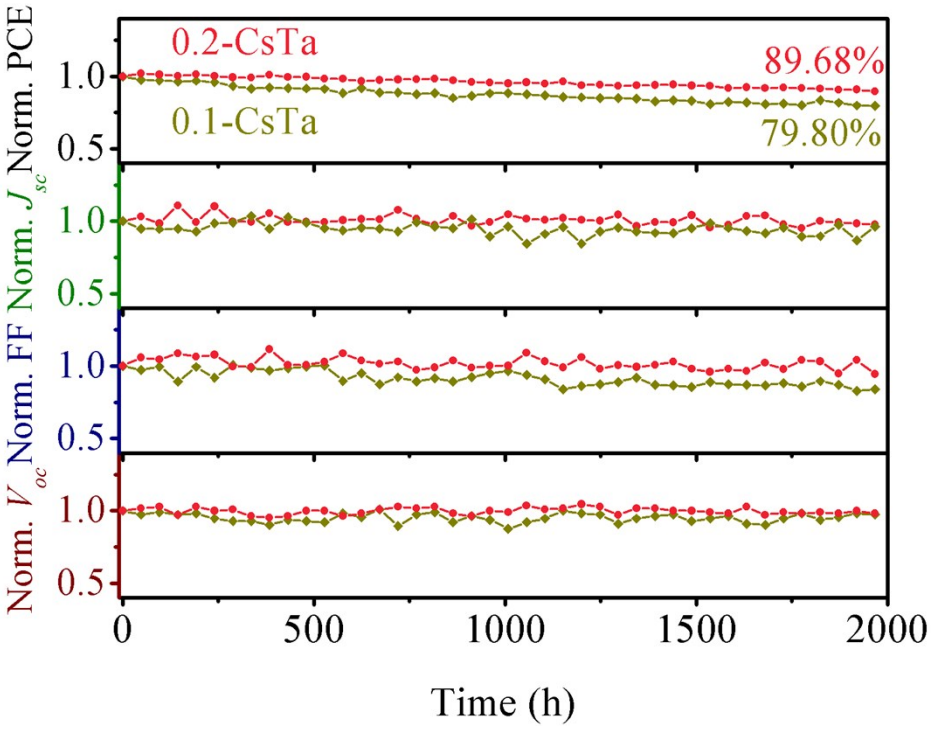

Figure S15. Photovoltaic parameter decays for 0.1-CsTa and 0.2-CsTa PSCs for environmental stability testing in air (RH: ~20%, RT: 10°C).

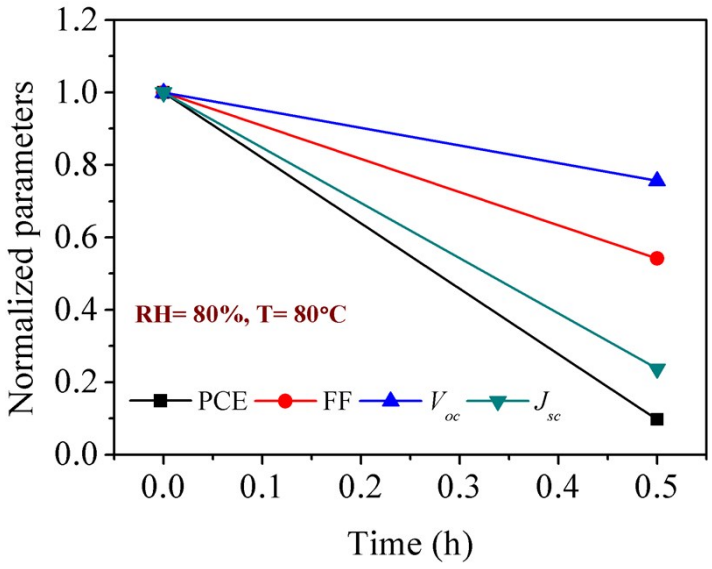

Figure S16. Photovoltaic parameter decays for PbI_2-prepared 0-CsTa PSCs for thermal stability testing under a RH=80% and T=80°C environment.

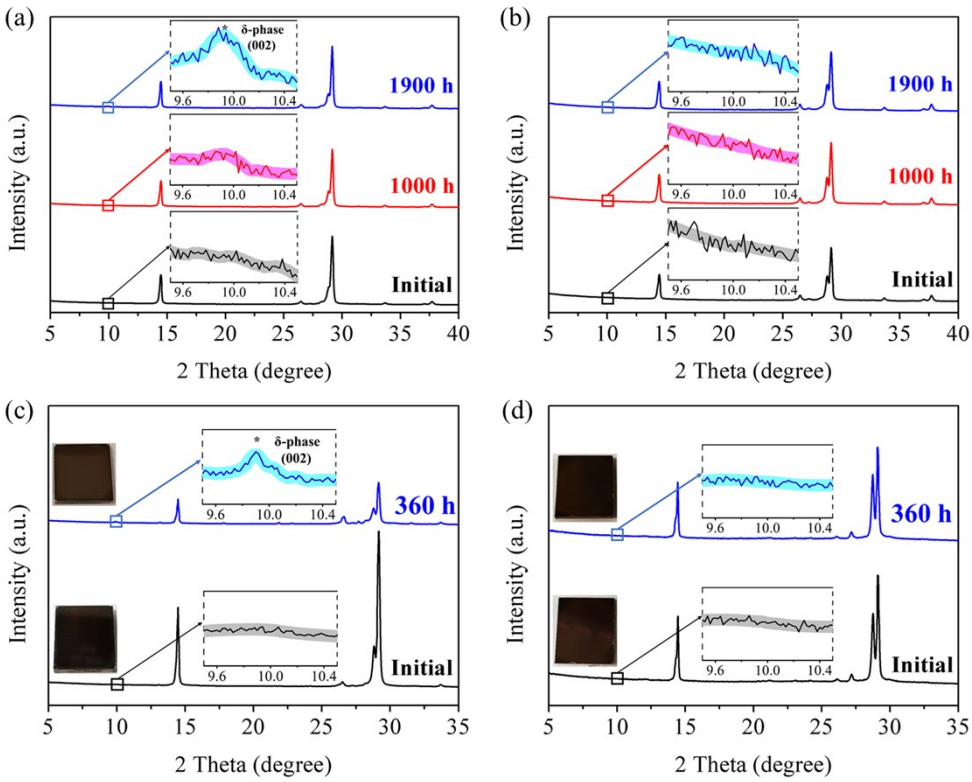

Figure S17. The XRD patterns for 0.1-CsTa and 0.2-CsTa perovskite films obtained under the same environment for stability tests. (a) 0.1-CsTa and (b) 0.2-CsTa perovskite films under a RH=~20% and T=10°C, environment for 1000 hours and 1900 hours. (c) 0.1-CsTa and (d) 0.2-CsTa perovskite films under a RH=80% and T=80°C environment before and after the same storage time of 360 hours.

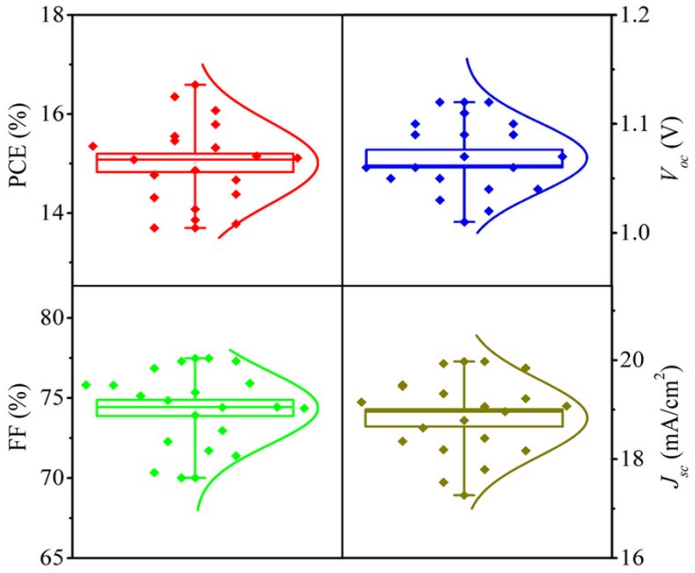

Figure S18. The statistical photoelectric parameters obtained for 0.1-CsTa PSCs based on the use of $HPbI_3$ as the lead source from measurements for 20 devices.

Table S1 Data obtained by fitting TRPL spectra for films without ETL based on 0-CsTa and 0.1-CsTa precursor solutions with an exponential decay function.

Samples	τ_1 (ns)	T_1 (%)	τ_2 (ns)	T_2 (%)	τ_3 (ns)	T_3 (%)	τ_{avg} (ns) [a]
0-CsTa	0.97	74.91	4.55	25.09	0	0	1.86
0.1-CsTa	1.33	9.31	27.30	25.35	156.35	65.34	109.20

[a] $\tau_{avg} = \sum_i A_i\tau_i, where \sum_i A_i = 1$.

Table S2 Photovoltaic parameters for PSCs based on n-CsTa PbI_2-based precursors

Samples n-CsTa	Scanning directions	J_{sc} [mA/cm^2]	V_{oc} [V]	FF [%]	PCE [%]	Hysteresis [%]
0-CsTa	R	13.18	0.85	67.63	7.61	41.65
	F	14.51	0.83	36.84	4.44	
0.1-CsTa	R	17.45	1.09	77.28	14.70	15.3
	F	17.36	1.09	65.68	12.45	
0.2-CsTa	R	15.68	1.09	69.06	11.85	17.0
	F	16.15	1.02	59.58	9.84	
0.3-CsTa	R	14.87	0.91	68.14	9.23	13.4
	F	14.65	0.83	65.04	7.94	

Table S3 Photovoltaic parameters of PSCs based on $HPbI_3$-prepared 0-CsTa and 0.1-CsTa precursor solutions.

Samples 0.1-CsTa	Scanning directions	J_{sc} [mA/cm^2]	V_{oc} [V]	FF [%]	PCE [%]
0-CsTa	R	19.23	1.05	75.43	15.25

	F	17.44	0.98	75.13	12.93
0.1-CsTa	R	19.48	1.10	77.30	16.59
	F	18.29	1.07	71.93	14.09

Table S4 Stability results obtained from representative studies for organic-added $CsPbI_3$ PSCs without encapsulation

Perovskite/Organic additives	PCE [%]	Storage environments and times	Remaining the initial PCE	Reference
$CsPbI_3$/zwitterion	11.4	RH: 30% 720 hours	85%	*Joule*, **2017**, 1(2): 371-382.
$CsPbI_3$/BAI	4.8	RH: 30% 720 hours	92%	*Journal of Materials Chemistry A*, **2017**, 5(5): 2066-2072.
$CsPbI_3$/EDAI	11.8	Dark dry air 720 hours	84.3%	*Science advances*, **2017**, 3(9): e1700841.
$CsPbI_3$/PEAI	5.7	Dry air 96 hours	75%	*Nanoscale*, **2018**, 10(14): 6318-6322.
$CsPbI_3$/PEAI	12.4	RH:20±5% 960 hours	83%	*Joule*, **2018**, 2(7): 1356-1368.
$CsPbI_3$/ PEAI	15.1	RH: 20-30% 1440 hours	92%	*Nature communica*

				tions, **2018**, 9(1): 1-8.
$CsPbI_3$/PVP	10.7	RH: 45-55% 500 hours	75%	*Nature communications*, **2018**, 9(1): 1-8.
$CsPbI_3$/DETAI	7.9	Dark dry air 1008 hours	92%	*Journal of Materials Chemistry A*, **2018**, 6(37): 18258-18266.
$CsPbI_3$/OTG3	13.2	Dark RH: ~10% 720 hours	85%	*Advanced materials*, **2019**, 31(24): 1900605.
$CsPbI_3$/MAI/MAS	16.04	Nitrogen 1000 hours	95%	*ACS Energy Letters*, **2020**, 5(5): 1619-1627.
$CsPbI_{2.84}Br_{0.16}$/0.1-CsTa (lead source: PbI_2)	14.70	RH: 80% Temperature:80^o C 360 hours	64.07%	This work
		RH: 20% 1008 hours/ 1968 hours	88.5%/ 79.8%	
$CsPbI_{2.84}Br_{0.16}$/0.2-CsTa	11.85	RH: 80%	87.4%	

(lead source: PbI_2)		Temperature:80^o C 500 hours		
		RH: 20% 1008 hours / 1968 hours	95.26%/ 89.68%	
$CsPbI_{2.84}Br_{0.16}$/0.1-CsTa (lead source: $HPbI_3$)	16.59	RH: 20% 1296 hours	80.88%	

Experimental sections

1. Precursor Solution Preparation

The CsTa added $CsPbI_{2.84}Br_{0.16}$ perovskite precursor solutions were prepared by using mole ratios of CsI: PbI_2: CsBr: CsTa= 1:1:0.4:n (n=0, 0.1, 0.2 and 0.3). m mol (m=0, 0.08, 0.16 and 0.24) CsTa, 0.8 mol cesium iodide (CsI, 99%) and 0.32 mol cesium bromide (CsBr, 99.99%) were dissolved with a 0.8 mol lead source into 1 ml DMSO to yield 0.8 M precursor solutions. The precursor solutions were stirred at 60 °C for 4 hours, and then filtered with a 0.25 μm nylon filter. The raw materials, PbI_2, CsBr, CsI and CsTa, were purchased from TCI. All the materials were used as received without further purification. $HPbI_3$ was synthesized by adding PbI_2 and 57 wt% hydroiodic acid with a molar ratio of 1:1.4 into DMF. The mixed solution was stirred for 2 h. The precipitate was then obtained by evaporating the solutions at 70 °C. The resulting solid was washed four times with copious diethyl ether until the supernatant turned colorless. Finally, the powders were dried in a vacuum oven at 50 °C.

2. Device Fabrication

The FTO was cleaned with detergent, deionized water, and ethanol. The cleaned substrate was then treated with UV ozone for 20 min. The compact TiO_2 (c-TiO_2) was fabricated by dipping the FTO into a 200 ml cold aqueous solution of 4.5 ml $TiCl_4$ at 70°C for 1 h. After that, the substrate was annealed at 200°C for 30 mins. The FTO/c-

TiO_2 was then treated with UV ozone for 20 min once more. Then, 45 μl perovskite precursor solutions were drop cast onto FTO/c-TiO_2 preheated to 90°C. Next, the wet films were immediately spun at 3000 rpm for 30 s, and then annealed at 60 °C for 3 min and 180 °C for 3 min. For the HTL, a solution of 72.3 mg spiro-MeOTAD, 17.5 mL of a prepared solution of 520 mg/mL lithium bis(trifluoromethylsulphonyl)imide, and 28.8 mL 4-tert-butylpyridine in 1 mL chlorobenzene was spun at 3000 rpm for 20 s. The devices were completed by depositing a 75 nm Au cathode by thermal evaporation under a pressure of 4 × 10−4 Pa. Both PbI_2 and $HPbI_3$-based devices were prepared by following the above fabrication processes except for the use of an annealing time of 20 min at 180°C for the $HPbI_3$-based devices.

3. Device Characterization

XRD patterns were obtained by using an X-ray diffractometer (SmartLab, Rigaku) with Cu Kα radiation (1.5418 Å). SEM images were taken with a SU8010 SEM (Hitachi). Absorption spectra were measured with a UV-2450 spectrophotometer (Shimadzu). The steady-state fluorescence and TRPL decay spectra were measured with a steady/transient state spectrophotometer (NanoLOG-TCSPC, USA) with an excitation wavelength of 450 nm. FTO with a sheet resistance of 15 Ω per square was obtained from Pilkington TEC. The active area of the solar cell was 0.09 cm^2, which was defined to be 0.09 cm^2 by using a black aperture mask. The $J-V$ curves were measured using a Keithley 2400 source meter together with a sunlight simulator (XES-300T1, SANEI Electric, AM 1.5 G), which was calibrated using a standard silicon reference cell (scan rate: 44 mV/s). The incident photon-to-electron conversion efficiency (IPCE) was measured in air using a QE-R measurement system (Enli Technology). The IR spectra were obtained with a Fourier-transform infrared spectrometer (Nicolet iS50, USA). Transient photovoltage decay measurements were performed using an electrochemical workstation (Zahner). X-ray photoelectron spectroscopy (XPS) was performed using an RBD upgraded PHI-5000C ESCA system (Perkin Elmer) with Mg Kα radiation (hμ = 1486.6 eV). The contact angles were collected by using a Dataphysics OCA15EC. EBSD tests were measured with a high-

performance field emission scanning electron microscope (Zeiss Merlin). TOF-SIMS was performed using a TOF-SIMS5 (ION-TOF GmbH, Germany) by utilizing a cesium-ion beam (Sput. Rate=0.23 nm/s).

4. DFT Calculation Methods

In this work, the density functional theory (DFT) calculation was performed using the Dmol^3 code.[1] The exchange-correlation interaction was treated by the generalized gradient approximation (GGA) with the PBE functional.[2] A double numerical quality basis set with d-type polarization function (DNP^3) was utilized for all the geometric optimizations, total energy calculations. The core electrons were modeled using effective core pseudopotentials (ECP) by Dolg[4] and Bergner[5]. All calculations were spin unrestricted. The positions of all the atoms were fully relaxed until the following convergence criterion were met: 0.002 Ha/Å for force, 10^{-5} Ha for total energy and 0.005 Å for displacement. The real space cutoff radius for complete vacancy formation was 5.5 Å. The self-consistent field computation criterion was chosen to be 10^{-6} Ha.

5. Space Charge Limited Current Methods

The trap density can be calculated from the following equation

$$V_{TFL} = \frac{en_t L^2}{2\varepsilon\varepsilon_0}$$

where L is the thickness of the perovskite film (≈480 nm), ε is the relative dielectric constant of the inorganic perovskite (taken as 18 from a previous report[6]), ε_0 is the vacuum permittivity (8.854×10^{-12} F/m), and e is the unit charge with a value of 1.602×10^{-19} C. n_t is the trap density.

Reference

1 Perdew, J. P., Burke, K. & Ernzerhof, M. Generalized Gradient Approximation Made Simple. *Phys Rev Lett* **77**, 3865-3868 (1996).

2 Delley, B. From molecules to solids with the DMol3 approach. *The Journal of*

Chemical Physics **113**, 7756-7764 (2000).

3 Delley, B. An all-electron numerical method for solving the local density functional for polyatomic molecules. *The Journal of chemical physics* **92**, 508-517 (1990).

4 Dolg, M., Wedig, U., Stoll, H. & Preuss, H. Energy-adjusted abinitio pseudopotentials for the first row transition elements. *The Journal of Chemical Physics* **86**, 866-872, doi:doi:http://dx.doi.org/10.1063/1.452288 (1987).

5 Bergner, A., Dolg, M., Küchle, W., Stoll, H. & Preuß, H. Ab initio energy-adjusted pseudopotentials for elements of groups 13–17. *Mol Phys* **80**, 1431-1441, doi:10.1080/00268979300103121 (1993).

6 Frost, J. M. Calculating polaron mobility in halide perovskites. *Physical Review B* **96**, 195202 (2017).